Search for Charged Higgs Bosons in e$^+$e$^-$ Collisions at Centre-of-Mass Energies between 130 and 183 GeV

The L3 Collaboration

Abstract

A search for pair-produced charged Higgs bosons is performed with the L3 detector at LEP using data collected at centre-of-mass energies from 130 to 183 GeV, corresponding to an integrated luminosity of 88.3 pb^{-1}. The Higgs decays into a charm and a strange quark or into a tau lepton and its associated neutrino are considered. The observed candidates are consistent with the expectations from Standard Model background processes. A lower limit of 57.5 GeV on the charged Higgs mass is derived at 95% CL, independent of the decay branching ratio Br(H$^\pm \to \tau\nu$).

Introduction

In the Standard Model [1], the Higgs mechanism [2] is used to generate the masses of W and Z bosons via spontaneous breaking of the local gauge symmetry. The Higgs sector requires one doublet of complex scalar fields which leads to the prediction of a single neutral scalar Higgs boson.

There are more general models, *e.g.* those derived from supersymmetry, that contain more than one Higgs doublet [3]. A minimal extension to the Standard Model has a two–doublet Higgs sector, which leads to five physical Higgs bosons: three neutral (A^0, h^0, H^0) and two charged ($H^\pm$). The discovery of a charged Higgs particle would be clear evidence for physics beyond the Standard Model.

Charged Higgs bosons can be produced in e^+e^- interactions via the process $e^+e^- \rightarrow (Z/\gamma) \rightarrow H^+H^-$. The Born cross section in the framework of two doublet models contains the mass of the charged Higgs boson as the only free parameter [4]. In this letter, we describe the analysis of the data taken at LEP from 1995 to 1997 at centre-of-mass energies between 130–183 GeV. The sensitivity of this data covers the Higgs mass region below the mass of the charged heavy gauge boson, m_W. Charged Higgs bosons are expected to decay mainly into the heaviest lepton that is kinematically allowed and its associated neutrino, or into the heaviest kinematically allowed quark pair whose decay is not Cabibbo–suppressed. Thus there are three possible decay modes: $H^+H^- \rightarrow \tau^+\nu_\tau\tau^-\bar{\nu}_\tau$, $c\bar{s}\tau^-\bar{\nu}_\tau$ and $c\bar{s}\bar{c}s$. The relative branching ratio is model dependent. Therefore three different analyses are optimised for each of the possible final states. The results include and supersede previous lower limits to the mass of charged Higgs bosons established by L3 using the data collected at the Z peak [5]. Results from other LEP experiments are published in Ref. [6].

Data Analysis

The data were collected with the L3 detector [7] at LEP, corresponding to an integrated luminosity of 88.3 pb^{-1}; where 12.0 pb^{-1} were collected at a centre-of-mass energy of 130–136 GeV, 10.8 pb^{-1} at 161 GeV, 10.2 pb^{-1} at 172 GeV and 55.3 pb^{-1} at 183 GeV.

The signal cross section is calculated using the PYTHIA Monte Carlo program [8]. For the efficiency estimates, samples of $e^+e^- \rightarrow (Z/\gamma) \rightarrow H^+H^-$ events are generated for Higgs masses between 40 and 80 GeV in mass steps of 5 GeV. About 1000 events for each final state are generated at each Higgs mass. For the background studies the following Monte Carlo generators are used: PYTHIA for $e^+e^- \rightarrow q\bar{q}(\gamma)$ and $e^+e^- \rightarrow ZZ$, KORALW [9] for $e^+e^- \rightarrow W^+W^-$, PHOJET [10] for $e^+e^- \rightarrow e^+e^-q\bar{q}$, DIAG36 [11] for $e^+e^- \rightarrow e^+e^-\ell^+\ell^-$ ($\ell = e, \mu, \tau$), KORALZ [12] for $e^+e^- \rightarrow \mu^+\mu^-$, $e^+e^- \rightarrow \tau^+\tau^-$ and BHAGENE3 [13] for $e^+e^- \rightarrow e^+e^-$. The L3 detector response is simulated using the GEANT program [14] which takes into account the effects of energy loss, multiple scattering and showering in the detector.

Search in the $H^+H^- \rightarrow \tau^+\nu_\tau\tau^-\bar{\nu}_\tau$ Channel

The signature for the leptonic decay channel is a pair of tau leptons with large missing energy and momentum, giving rise to low multiplicity events with low visible energy. Such events are selected by requiring a visible energy of less than $0.5\sqrt{s}$, between 2 and 20 calorimetric clusters and a charged track multiplicity of between 2 and 8. Dilepton final states from $e^+e^- \rightarrow \ell^+\ell^-$ ($\ell = e, \mu, \tau$) are rejected by requiring the maximum angle between any pair of tracks to be less

m$_{H^\pm}$ (GeV)	$\sqrt{s}$ (GeV)			
	130-136	161	172	183
45	29	20	21	23
50	33	22	23	25
55	35	24	26	26
60	38	27	29	27
65	-	28	29	28
70	-	30	30	30

Table 1: Selection efficiencies (in %) for the $\tau^+\nu_\tau\tau^-\bar{\nu}_\tau$ final state for different masses m$_{H^\pm}$ at different centre-of-mass energies.

than 165° and the event thrust to be less than 0.98. Radiative dilepton production is reduced by rejecting events with one or more reconstructed photons with energy greater than 20 GeV. Background from two-photon interactions is reduced by rejecting events where the sum of the energy deposited in the luminosity monitor and the active lead rings exceeds 1 GeV. Remaining two-photon interaction events are rejected by requiring the energy imbalance transverse and parallel to the beam axis to be greater than 0.2 and less than 0.7 respectively, and by rejecting events where there is no reconstructed jet with a momentum transverse to the beam axis exceeding 15 GeV. Cosmic muons are rejected by requiring tracks to originate from the e$^+$e$^-$ interaction region and at least one scintillator hit in time with the beam crossing.

Tau leptons are identified via their decay into isolated electrons or muons, or as a narrow hadronic jet. Muons must have a momentum of at least 5% of the beam energy in order to reduce the number of fake signatures from hadrons that escape the hadron calorimeter. For hadronically decaying τ candidates, the ratio E$_{30}$/E$_{10}$ must be less than 1.3, where E$_{30}$ and E$_{10}$ are the energy depositions in a 30° and 10° half angle cone around the direction of the decay particles of the τ respectively.

Events that are consistent with the signal are selected by requiring the presence of at least two τ decay candidates. At centre-of-mass energies above 136 GeV, additional criteria are applied to the τ candidates to reduce contamination from WW $\rightarrow$ q$\bar{q}\ell\nu$ ($\ell =$ e, μ). More energetic leptons are more likely to come directly from a W decay than from a charged Higgs because of the greater number of unobserved neutrinos in the latter case. For τ decays to electrons or muons, the observed lepton energy must be less than 0.45 of the beam energy (Figure 1). Further reduction of W background is achieved by requiring the event to have at least one hadronically decaying τ candidate.

The efficiency of the H$^+$H$^- \rightarrow \tau^+\nu_\tau\tau^-\bar{\nu}_\tau$ selection for the different Higgs masses is shown in Table 1. Table 2 shows the number of events selected in the data and the expected background for the different centre-of-mass energies. The total number of events selected in data is 7, where 11.3 background events are expected from Standard Model processes. Almost all of the remaining background comes from W pair production.

Systematic uncertainties in the signal efficiencies and the expected number of background events were investigated by comparing the distributions of several signal-sensitive variables in the data and the Monte Carlo. We assign a systematic error of 0.8 events in the total predicted background and 1.5% in the expected signal efficiencies.

$\sqrt{s}$ (GeV)	130–136	161	172	183
Expected background	0.3	0.5	1.3	9.2
Data	0	0	1	6

Table 2: Expected background and number of events selected in data in the $\tau^+\nu_\tau\tau^-\bar{\nu}_\tau$ final state at each centre-of-mass energy.

Search in the $\mathrm{H^+H^-} \to \mathrm{c\bar{s}}\tau^-\bar{\nu}_\tau$ Channel

The semileptonic final state $\mathrm{H^+H^-} \to \mathrm{c\bar{s}}\tau^-\bar{\nu}_\tau$[1] is characterised by two hadronic jets, a τ lepton and missing momentum. High multiplicity events are selected by requiring more than 5 charged tracks and more than 10 calorimetric clusters. Tau leptons are identified in the same way as for the $\mathrm{H^+H^-} \to \tau^+\nu_\tau\tau^-\bar{\nu}_\tau$ selection with the additional constraint that hadronically decaying τ candidates must have one or three tracks and unit charge. Selected events are forced into two jets using the DURHAM algorithm [15], after subtracting the τ candidate.

The kinematic cuts differ slightly for the different centre-of-mass energies. As an example, we describe here the cuts for the $\sqrt{s} = 183$ GeV data where we have the largest search sensitivity due to the high centre-of-mass energy and the large integrated luminosity.

The missing transverse momentum must be at least 10% of the visible energy in order to reject background from the reactions $\mathrm{e^+e^-} \to \mathrm{q\bar{q}q\bar{q}}(\gamma)$ and $\mathrm{q\bar{q}}(\gamma)$ (Figure 2a). The background contribution from $\mathrm{e^+e^-} \to \mathrm{q\bar{q}}(\gamma)$ is further reduced by requiring the missing momentum parallel to the beam axis to be smaller than 50% of the visible energy. The polar angle of the missing momentum vector must satisfy $|\cos\Theta_{\mathrm{miss}}| < 0.9$. Furthermore, the visible mass, after subtraction of the τ candidate, must be less than 90 GeV and the opening angle of the two jets must be less than 160° in the plane perpendicular to the beam axis. The energy deposition in a cone of 25° around the missing momentum vector projected in the same plane must be smaller than 40 GeV and the sum of the opening angles of the τ candidate and the missing momentum vector to the closest jet is required to be larger than 80°.

A kinematic fit is performed imposing energy and momentum conservation for an assumed production of a pair of equal mass particles with one decaying into two jets and the other into a τ and a neutrino. The directions of the jets, of the τ and of the missing momentum vector are kept at their measured values. Using this method, a resolution of about 4 GeV is obtained in the distribution of the effective mass of the two jets and of the τ and the neutrino.

Semileptonically decaying W-pairs ($\mathrm{WW} \to \mathrm{q\bar{q}}\ell\nu; \ell = \mathrm{e}, \mu$) are suppressed in the following way: the four momenta are transformed into the rest frame of the leptonically decaying parent particle. In this frame, the lepton energy E^*_ℓ is greater if the lepton comes from a prompt W decay than from a τ decay. The missing momentum $|\mathrm{P}^*_{\mathrm{miss}}|$ is also larger in the first case because the neutrinos from the τ decay are almost oppositely directed to the τ neutrino coming directly from the W. For the selection, the sum $\mathrm{E}^*_\ell + |\mathrm{P}^*_{\mathrm{miss}}|$ is used, which should be smaller than 60 GeV for an electron and smaller than 50 GeV for a muon in the final state. The discriminating power of this variable is shown in Figure 2b.

To further reject $\mathrm{q\bar{q}}(\gamma)$, two–photon interactions and W pair events, the flight direction of the parent particle is considered. The production of the charged Higgs follows a $\sin^2\Theta$ dependance whereas the major fraction of the background is collected in the forward-backward region of

---

[1] The charge conjugated decay is also considered.

m$_{H\pm}$ (GeV)	$\sqrt{s}$ (GeV) 130–136	161	172	183
45	41	36	34	38
50	41	40	35	41
55	39	42	46	42
60	33	47	46	41
65	—	44	44	42
70	—	41	42	42

Table 3: Selection efficiencies (in %) for the $c\bar{s}\tau^-\bar{\nu}_\tau$ final state for different masses m$_{H\pm}$ at different centre-of-mass energies.

$\sqrt{s}$ (GeV)	130–136	161	172	183
Expected background	0.6	2.0	7.1	30.1
Data	1	1	9	28

Table 4: Background expectation and observed data at the investigated centre-of-mass energies for the $c\bar{s}\tau^-\bar{\nu}_\tau$ channel.

the detector (Figure 2c). Events with $\mid \cos\Theta \mid \leq 0.9$ are accepted.

The selection efficiencies for the different centre-of-mass energies are shown in Table 3. The background expectation together with the selected data events are given in Table 4. The total number of events selected in data is 39, where 39.8 background events are expected from Standard Model processes. The background is dominated by the process WW$\rightarrow$ q$\bar{\text{q}}\tau\nu$ ($\approx 70\%$) and other WW decays ($\approx 22\%$); the remaining contributions are q$\bar{\text{q}}(\gamma)$ and neutral current four-fermion events. For the final mass distribution, we use the average of the masses of the jet–jet and the $\tau\,\nu$ pairs respectively, calculated after the kinematic fit. Figure 2d shows the mass distribution for data and background events for all investigated centre-of-mass energies combined.

The main contribution to the systematic error comes from the τ identification. Systematic uncertainties in the τ identification were studied using high statistic e$^+$e$^-$ $\rightarrow$ e$^+$e$^-$, e$^+$e$^-$ $\rightarrow$ $\mu^+\mu^-$, e$^+$e$^-$ $\rightarrow$ $\tau^+\tau^-$ and e$^+$e$^-$ $\rightarrow$ q$\bar{\text{q}}(\gamma)$ data and MC samples at 91 GeV centre-of-mass energy. A systematic error of 2% for the signal efficiency and 2.5% for the background expectation is derived.

Search in the H$^+$H$^-$ $\rightarrow$ c$\bar{\text{s}}\bar{\text{c}}$s Channel

Events of the channel H$^+$H$^-$ $\rightarrow$ c$\bar{\text{s}}\bar{\text{c}}$s have high multiplicity and are balanced in transverse and longitudinal momenta. Their total centre-of-mass energy is deposited in the detector and they are characterized by four hadronic jets. The cut values differ slightly at the different centre-of-mass energies. The cuts described here are for $\sqrt{s} = 183$ GeV.

Candidate events are selected by requiring more than 15 charged tracks and more than 45 calorimetric clusters. The visible energy must be between $0.6\sqrt{s}$ and $1.4\sqrt{s}$ and the transverse and longitudinal normalised missing energy less than 0.3.

Radiative q$\bar{\text{q}}(\gamma)$ events are suppressed by rejecting events that contain an isolated photon with an energy greater $0.1\sqrt{s}$. Furthermore, the event spherocity must be within 0.14 and 0.74.

The events are subject to the DURHAM algorithm with $Y_{34} = 0.008$. Events with less than 4 jets are rejected and the remaining ones are forced into four jets. The jet energies are rescaled with a common factor so that their sum is equal to $\sqrt{s}$.

The four jets are grouped into three possible pairings and the differences between the invariant masses of all pairings are calculated. Choosing the pair with the minimum invariant mass difference, the polar angle of the parent particle must satisfy $|\cos\Theta| < 0.8$. The opening angle between the two jets originating from the same parent particle must be between 53° and 130°. Considering the jet pairing with the medium invariant mass difference, events are rejected if the average of the two masses is within 2 GeV equal to m_W and their difference is less than 20 GeV. With these cuts the number of WW events is further reduced.

A five-constraint kinematic fit is then applied assuming the production of a pair of equal mass particles each decaying into two jets. The χ^2 per degree-of-freedom of the fit must be smaller than 5.5. This further suppresses the $q\bar{q}$ background.

The selection efficiencies are shown in Table 5. The expected background and the selected data are shown in Table 6. The total number of events selected in data is 145, where 159.5 background events are expected from Standard Model processes. The main contribution to the background comes from W pair decays into four jets. In Figure 3, the average dijet invariant mass distribution is shown for the data and the expected background at $\sqrt{s} = 130 - 183$ GeV. The low mass tail for the WW background is due to incorrectly assigned jet pairs.

Systematic errors are assigned to the signal efficiencies and the expected number of background events by comparing the distributions of signal-sensitive variables in the data and the Monte Carlo simulation. The main contribution to the systematic error comes from the fact that the number of reconstructed jets per event is not perfectly simulated in the Monte Carlo. We assign a systematic error of 4.5 events in the total predicted background and 0.6% in the expected signal efficiencies.

	$\sqrt{s}$ (GeV)			
$m_{H^\pm}$ (GeV)	130–136	161	172	183
45	36	37	35	29
50	41	45	45	36
55	44	51	45	39
60	46	44	43	40
65	–	45	41	38
70	–	46	39	34

Table 5: Selection efficiencies (in %) for the $c\bar{s}\bar{c}s$ final state for different masses $m_{H^\pm}$ at different centre-of-mass energies.

$\sqrt{s}$ (GeV)	130–136 GeV	161 GeV	172 GeV	183 GeV
Expected background	19.0	15.2	25.9	99.4
Data	21	13	18	93

Table 6: Expected background and number of events selected in data in the $c\bar{s}\bar{c}s$ final state at each centre-of-mass energy.

Results

The number of selected events in data is consistent, in each decay channel, with the number of events expected from Standard Model processes. No indication of pair-produced charged Higgs bosons is observed. Mass limits as a function of the branching fraction $Br(H^{\pm} \to \tau\nu)$ are derived at 95% confidence level, where the confidence level is calculated using the same technique described in Reference [16]. For the $H^+H^- \to c\bar{s}\bar{c}s$ and the $H^+H^- \to c\bar{s}\tau^-\bar{\nu}_{\tau}$ channels we use the reconstructed mass distribution in the limit calculation, whereas for the $H^+H^- \to \tau^+\nu_{\tau}\tau^-\bar{\nu}_{\tau}$ channel the total number of data, expected background and expected signal events are used.

Systematic uncertainties are taken into account using the same procedure as in the Standard Model Higgs search [17]. In addition to the systematic errors resulting from the selection, an error of 0.3% on the luminosity measurement, an error of 5% on the background normalisation and an error of 2% on the signal cross section are taken into account.

Figure 4 shows the excluded mass regions of charged Higgs bosons at 95% CL for the analyses of each final state and their combination as function of the branching fraction $Br(H^{\pm} \to \tau\nu)$. A lower limit on the mass of the charged Higgs boson of

$$m_{H^{\pm}} > 57.5 \text{ GeV} \tag{1}$$

independent of the branching fraction is obtained.

Acknowledgements

References

[1] S.L. Glashow, Nucl. Phys. **22** (1961) 579;
S. Weinberg, Phys. Rev. Lett. **19** (1967) 1264;
A. Salam, "Elementary Particle Theory", eds. N. Svartholm, Stockholm, "Almquist and Wiksell" (1968), 367.

[2] P. W. Higgs, Phys. Lett. **12** (1964) 132, Phys. Rev. Lett. **13** (1964) 508 and Phys. Rev. **145** (1966) 1156;
F. Englert and R. Brout, Phys. Rev. Lett. **13** (1964) 321;
G.S. Guralnik *et* al, Phys. Rev. Lett. **13** (1964) 585.

[3] S. Dawson, J.F. Gunion, H.E. Haber and G.L. Kane, The Physics of the Higgs Bosons: Higgs Hunter's Guide, Addison Wesley, Menlo Park, 1989.

[4] H. Baer *et al*, CERN 86-02, CERN Yellow Report, eds John Ellis and Roberto Peccei, Vol.1, 297.

[5] L3 Collab., O. Adriani *et al.*, Phys. Lett. **B 294** (1992) 457;
L3 Collab., O. Adriani *et al.*, Z. Phys. **C 57** (1993) 355.

[6] ALEPH Collab., R. Barate *et al*, Phys. Lett. **B 418** (1998) 419;
DELPHI Collab., P. Abreu *et al*, Phys. Lett. **B 420** (1998) 140;
OPAL Collab., K. Ackerstaff *et al*, Phys. Lett. **B 426** (1998) 180.

[7] L3 Collaboration, B. Adeva *et al*, Nucl.Instr.Meth. **A289** (1990) 35;
J.A. Bakken *et al*, Nucl.Instr.Meth. **A275** (1989) 81;
O. Adriani *et al*, Nucl.Instr.Meth. **A302** (1991) 53;
B. Adeva *et al*, Nucl.Instr.Meth. **A323** (1992) 109;
K. Deiters *et al*, Nucl.Instr.Meth. **A323** (1992) 162;
M. Chemarin *et al*, Nucl.Instr.Meth. **A349** (1994) 345;
B. Acciari *et al*, Nucl.Instr.Meth. **A351** (1994) 300;
G. Basti *et al*, Nucl.Instr.Meth. **A374** (1996) 293;
A. Adam *et al*, Nucl.Instr.Meth. **A383** (1996) 342.

[8] T. Sjöstrand, CERN-TH 7112/93, CERN (1993), revised August 1995;
T. Sjöstrand, Comp. Phys. Comm. **82** (1994) 74.

[9] M. Skrzypek *et al.*, Comp. Phys. Comm. **94** (1996) 216;
M. Skrzypek *et al.*, Phys. Lett. **B372** (1996) 289.

[10] R. Engel, Z. Phys. **C 66** (1995) 203;
R. Engel and J. Ranft, Phys. Rev. **D 54** (1996) 4244.

[11] F.A. Berends, P.H. Daverfeldt and R. Kleiss, Nucl. Phys. **B 253** (1985) 441.

[12] S. Jadach, B.F.L. Ward and Z. Wąs, Comp. Phys. Comm. **79** (1994) 503.

[13] J.H. Field, Phys. Lett. **B 323** (1994) 432;
J.H. Field and T. Riemann, Comp. Phys. Comm. **94** (1996) 53.

[14] The L3 detector simulation is based on GEANT Version 3.15.
See R. Brun *et al.*, "GEANT 3", CERN DD/EE/84-1 (Revised), September 1987.
The GHEISHA program (H. Fesefeldt, RWTH Aachen Report PITHA 85/02 (1985)) is used to simulate hadronic interactions.

[15] S. Bethke *et al.*, Nucl. Phys. **B 370** (1992) 310.

[16] L3 Collaboration, M. Acciari *et al.*, Phys.Lett. **B411** (1997) 373.

[17] L3 Collaboration, M. Acciari *et al.*, Phys.Lett. **B431** (1998) 437.

The L3 Collaboration:

M.Acciarri,[28] O.Adriani,[17] M.Aguilar-Benitez,[27] S.Ahlen,[12] J.Alcaraz,[27] G.Alemanni,[23] J.Allaby,[18] A.Aloisio,[30] M.G.Alviggi,[30] G.Ambrosi,[20] H.Anderhub,[49] V.P.Andreev,[7,38] T.Angelescu,[14] F.Anselmo,[10] A.Arefiev,[29] T.Azemoon,[3] T.Aziz,[11] P.Bagnaia,[37] L.Baksay,[44] S.Banerjee,[11] Sw.Banerjee,[11] K.Banicz,[46] A.Barczyk,[49,47] R.Barillère,[18] L.Barone,[37] P.Bartalini,[23] A.Baschirotto,[28] M.Basile,[10] R.Battiston,[34] A.Bay,[23] F.Becattini,[17] U.Becker,[16] F.Behner,[49] J.Berdugo,[27] P.Berges,[16] B.Bertucci,[34] B.L.Betev,[49] S.Bhattacharya,[11] M.Biasini,[34] A.Biland,[49] G.M.Bilei,[34] J.J.Blaising,[4] S.C.Blyth,[35] G.J.Bobbink,[2] R.Bock,[1] A.Böhm,[1] L.Boldizsar,[15] B.Borgia,[18,37] D.Bourilkov,[49] M.Bourquin,[20] S.Braccini,[20] J.G.Branson,[40] V.Brigljevic,[49] I.C.Brock,[35] A.Buffini,[17] A.Buijs,[45] J.D.Burger,[16] W.J.Burger,[34] J.Busenitz,[44] A.Button,[3] X.D.Cai,[16] M.Campanelli,[49] M.Capell,[16] G.Cara Romeo,[10] G.Carlino,[30] A.M.Cartacci,[17] J.Casaus,[27] G.Castellini,[17] F.Cavallari,[37] N.Cavallo,[30] C.Cecchi,[20] M.Cerrada,[27] F.Cesaroni,[24] M.Chamizo,[27] Y.H.Chang,[51] U.K.Chaturvedi,[19] M.Chemarin,[26] A.Chen,[51] G.Chen,[8] G.M.Chen,[8] H.F.Chen,[21] H.S.Chen,[8] X.Chereau,[4] G.Chiefari,[30] C.Y.Chien,[5] L.Cifarelli,[39] F.Cindolo,[10] C.Civinini,[17] I.Clare,[16] R.Clare,[16] G.Coignet,[4] A.P.Colijn,[2] N.Colino,[27] S.Costantini,[9] F.Cotorobai,[14] B.de la Cruz,[27] A.Csilling,[15] T.S.Dai,[16] R.D'Alessandro,[17] R.de Asmundis,[30] A.Degré,[4] K.Deiters,[47] D.della Volpe,[30] P.Denes,[36] F.DeNotaristefani,[37] M.Diemoz,[37] D.van Dierendonck,[2] F.Di Lodovico,[49] C.Dionisi,[18,37] M.Dittmar,[49] A.Dominguez,[40] A.Doria,[30] M.T.Dova,[19,‡] D.Duchesneau,[4] P.Duinker,[2] I.Duran,[41] S.Easo,[34] H.El Mamouni,[26] A.Engler,[35] F.J.Eppling,[16] F.C.Erné,[2] P.Extermann,[20] M.Fabre,[47] R.Faccini,[37] M.A.Falagan,[27] S.Falciano,[37] A.Favara,[17] J.Fay,[26] O.Fedin,[38] M.Felcini,[49] T.Ferguson,[35] F.Ferroni,[37] H.Fesefeldt,[1] E.Fiandrini,[34] J.H.Field,[20] F.Filthaut,[18] P.H.Fisher,[16] I.Fisk,[40] G.Forconi,[16] L.Fredj,[20] K.Freudenreich,[49] C.Furetta,[28] Yu.Galaktionov,[29,16] S.N.Ganguli,[11] P.Garcia-Abia,[6] M.Gataullin,[33] S.S.Gau,[13] S.Gentile,[37] N.Gheordanescu,[14] S.Giagu,[37] S.Goldfarb,[23] J.Goldstein,[12] Z.F.Gong,[21] A.Gougas,[5] G.Gratta,[33] M.W.Gruenewald,[9] R.van Gulik,[2] V.K.Gupta,[36] A.Gurtu,[11] L.J.Gutay,[46] D.Haas,[6] B.Hartmann,[1] A.Hasan,[31] D.Hatzifotiadou,[10] T.Hebbeker,[9] A.Hervé,[18] P.Hidas,[15] J.Hirschfelder,[35] W.C.van Hoek,[32] H.Hofer,[49] H.Hoorani,[35] S.R.Hou,[51] G.Hu,[5] I.Iashvili,[48] B.N.Jin,[8] L.W.Jones,[3] P.de Jong,[18] I.Josa-Mutuberria,[27] R.A.Khan,[19] D.Kamrad,[48] J.S.Kapustinsky,[25] M.Kaur,[19,◊] M.N.Kienzle-Focacci,[20] D.Kim,[37] D.H.Kim,[43] J.K.Kim,[43] S.C.Kim,[43] W.W.Kinnison,[25] A.Kirkby,[33] D.Kirkby,[33] J.Kirkby,[18] D.Kiss,[15] W.Kittel,[32] A.Klimentov,[16,29] A.C.König,[32] A.Kopp,[48] I.Korolko,[29] V.Koutsenko,[16,29] R.W.Kraemer,[35] W.Krenz,[1] A.Kunin,[16,29] P.Lacentre,[48,♮,‡] P.Ladron de Guevara,[27] I.Laktineh,[26] G.Landi,[17] C.Lapoint,[16] K.Lassila-Perini,[49] P.Laurikainen,[22] A.Lavorato,[39] M.Lebeau,[18] A.Lebedev,[16] P.Lebrun,[26] P.Lecomte,[49] P.Lecoq,[18] P.Le Coultre,[49] H.J.Lee,[9] J.M.Le Goff,[18] R.Leiste,[48] E.Leonardi,[37] P.Levtchenko,[38] C.Li,[21] C.H.Lin,[51] W.T.Lin,[51] F.L.Linde,[2,18] L.Lista,[30] Z.A.Liu,[8] W.Lohmann,[48] E.Longo,[37] W.Lu,[33] Y.S.Lu,[8] K.Lübelsmeyer,[1] C.Luci,[18,37] D.Luckey,[16] L.Luminari,[37] W.Lustermann,[49] W.G.Ma,[21] M.Maity,[11] G.Majumder,[11] L.Malgeri,[18] A.Malinin,[29] C.Maña,[27] D.Mangeol,[32] P.Marchesini,[49] G.Marian,[44,¶] A.Marin,[12] J.P.Martin,[26] F.Marzano,[37] G.G.G.Massaro,[2] K.Mazumdar,[11] R.R.McNeil,[7] S.Mele,[18] L.Merola,[30] M.Meschini,[17] W.J.Metzger,[32] M.von der Mey,[1] D.Migani,[10] A.Mihul,[14] A.J.W.van Mil,[32] H.Milcent,[18] G.Mirabelli,[37] J.Mnich,[18] P.Molnar,[9] B.Monteleoni,[17] R.Moore,[3] T.Moulik,[11] R.Mount,[33] G.S.Muanza,[26] F.Muheim,[20] A.J.M.Muijs,[2] S.Nahn,[16] M.Napolitano,[30] F.Nessi-Tedaldi,[49] H.Newman,[33] T.Niessen,[1] A.Nippe,[23] A.Nisati,[37] H.Nowak,[48] Y.D.Oh,[43] G.Organtini,[37] R.Ostonen,[22] C.Palomares,[27] D.Pandoulas,[1] S.Paoletti,[37,18] P.Paolucci,[30] H.K.Park,[35] I.H.Park,[43] G.Pascale,[37] G.Passaleva,[18] S.Patricelli,[30] T.Paul,[13] M.Pauluzzi,[34] C.Paus,[18] F.Pauss,[49] D.Peach,[18] M.Pedace,[37] Y.J.Pei,[1] S.Pensotti,[28] D.Perret-Gallix,[4] B.Petersen,[32] S.Petrak,[9] A.Pevsner,[5] D.Piccolo,[30] M.Pieri,[17] P.A.Piroué,[36] E.Pistolesi,[28] V.Plyaskin,[29] M.Pohl,[49] V.Pojidaev,[29,17] H.Postema,[16] J.Pothier,[18] N.Produit,[20] D.Prokofiev,[38] J.Quartieri,[39] G.Rahal-Callot,[49] N.Raja,[11] P.G.Rancoita,[28] M.Rattaggi,[28] G.Raven,[40] P.Razis,[31] D.Ren,[49] M.Rescigno,[37] S.Reucroft,[13] T.van Rhee,[45] S.Riemann,[48] K.Riles,[3] A.Robohm,[49] J.Rodin,[44] B.P.Roe,[3] L.Romero,[27] S.Rosier-Lees,[4] S.Roth,[1] J.A.Rubio,[18] D.Ruschmeier,[9] H.Rykaczewski,[49] S.Sakar,[37] J.Salicio,[18] E.Sanchez,[27] M.P.Sanders,[32] M.E.Sarakinos,[22] C.Schäfer,[1] V.Schegelsky,[38] S.Schmidt-Kaerst,[1] D.Schmitz,[1] N.Scholz,[49] H.Schopper,[50] D.J.Schotanus,[32] J.Schwenke,[1] G.Schwering,[1] C.Sciacca,[30] D.Sciarrino,[20] L.Servoli,[34] S.Shevchenko,[33] N.Shivarov,[42] V.Shoutko,[29] J.Shukla,[25] E.Shumilov,[29] A.Shvorob,[33] T.Siedenburg,[1] D.Son,[43] B.Smith,[16] P.Spillantini,[17] M.Steuer,[16] D.P.Stickland,[36] A.Stone,[7] H.Stone,[36] B.Stoyanov,[42] A.Straessner,[1] K.Sudhakar,[11] G.Sultanov,[19] L.Z.Sun,[21] G.F.Susinno,[20] H.Suter,[49] J.D.Swain,[19] Z.Szillasi,[44,¶] X.W.Tang,[8] L.Tauscher,[6] L.Taylor,[13] C.Timmermans,[32] Samuel C.C.Ting,[16] S.M.Ting,[16] S.C.Tonwar,[11] J.Tóth,[15] C.Tully,[36] K.L.Tung,[8] Y.Uchida,[16] J.Ulbricht,[49] E.Valente,[37] G.Vesztergombi,[15] I.Vetlitsky,[29] G.Viertel,[49] S.Villa,[13] M.Vivargent,[4] S.Vlachos,[6] H.Vogel,[35] H.Vogt,[48] I.Vorobiev,[18,29] A.A.Vorobyov,[38] A.Vorvolakos,[31] M.Wadhwa,[6] W.Wallraff,[1] J.C.Wang,[16] X.L.Wang,[21] Z.M.Wang,[21] A.Weber,[1] S.X.Wu,[16] S.Wynhoff,[1] J.Xu,[12] Z.Z.Xu,[21] B.Z.Yang,[21] C.G.Yang,[8] H.J.Yang,[8] M.Yang,[8] J.B.Ye,[21] S.C.Yeh,[52] J.M.You,[35] An.Zalite,[38] Yu.Zalite,[38] P.Zemp,[49] Y.Zeng,[1] Z.P.Zhang,[21] B.Zhou,[12] G.Y.Zhu,[8] R.Y.Zhu,[33] A.Zichichi,[10,18,19] F.Ziegler,[48] G.Zilizi.[44,¶]

9

 1 I. Physikalisches Institut, RWTH, D-52056 Aachen, FRG[§]
     III. Physikalisches Institut, RWTH, D-52056 Aachen, FRG[§]
 2 National Institute for High Energy Physics, NIKHEF, and University of Amsterdam, NL-1009 DB Amsterdam,
     The Netherlands
 3 University of Michigan, Ann Arbor, MI 48109, USA
 4 Laboratoire d'Annecy-le-Vieux de Physique des Particules, LAPP,IN2P3-CNRS, BP 110, F-74941
     Annecy-le-Vieux CEDEX, France
 5 Johns Hopkins University, Baltimore, MD 21218, USA
 6 Institute of Physics, University of Basel, CH-4056 Basel, Switzerland
 7 Louisiana State University, Baton Rouge, LA 70803, USA
 8 Institute of High Energy Physics, IHEP, 100039 Beijing, China[△]
 9 Humboldt University, D-10099 Berlin, FRG[§]
10 University of Bologna and INFN-Sezione di Bologna, I-40126 Bologna, Italy
11 Tata Institute of Fundamental Research, Bombay 400 005, India
12 Boston University, Boston, MA 02215, USA
13 Northeastern University, Boston, MA 02115, USA
14 Institute of Atomic Physics and University of Bucharest, R-76900 Bucharest, Romania
15 Central Research Institute for Physics of the Hungarian Academy of Sciences, H-1525 Budapest 114, Hungary[‡]
16 Massachusetts Institute of Technology, Cambridge, MA 02139, USA
17 INFN Sezione di Firenze and University of Florence, I-50125 Florence, Italy
18 European Laboratory for Particle Physics, CERN, CH-1211 Geneva 23, Switzerland
19 World Laboratory, FBLJA Project, CH-1211 Geneva 23, Switzerland
20 University of Geneva, CH-1211 Geneva 4, Switzerland
21 Chinese University of Science and Technology, USTC, Hefei, Anhui 230 029, China[△]
22 SEFT, Research Institute for High Energy Physics, P.O. Box 9, SF-00014 Helsinki, Finland
23 University of Lausanne, CH-1015 Lausanne, Switzerland
24 INFN-Sezione di Lecce and Universitá Degli Studi di Lecce, I-73100 Lecce, Italy
25 Los Alamos National Laboratory, Los Alamos, NM 87544, USA
26 Institut de Physique Nucléaire de Lyon, IN2P3-CNRS,Université Claude Bernard, F-69622 Villeurbanne, France
27 Centro de Investigaciones Energeticas, Medioambientales y Tecnologicas, CIEMAT, E-28040 Madrid, Spain[♭]
28 INFN-Sezione di Milano, I-20133 Milan, Italy
29 Institute of Theoretical and Experimental Physics, ITEP, Moscow, Russia
30 INFN-Sezione di Napoli and University of Naples, I-80125 Naples, Italy
31 Department of Natural Sciences, University of Cyprus, Nicosia, Cyprus
32 University of Nijmegen and NIKHEF, NL-6525 ED Nijmegen, The Netherlands
33 California Institute of Technology, Pasadena, CA 91125, USA
34 INFN-Sezione di Perugia and Universitá Degli Studi di Perugia, I-06100 Perugia, Italy
35 Carnegie Mellon University, Pittsburgh, PA 15213, USA
36 Princeton University, Princeton, NJ 08544, USA
37 INFN-Sezione di Roma and University of Rome, "La Sapienza", I-00185 Rome, Italy
38 Nuclear Physics Institute, St. Petersburg, Russia
39 University and INFN, Salerno, I-84100 Salerno, Italy
40 University of California, San Diego, CA 92093, USA
41 Dept. de Fisica de Particulas Elementales, Univ. de Santiago, E-15706 Santiago de Compostela, Spain
42 Bulgarian Academy of Sciences, Central Lab. of Mechatronics and Instrumentation, BU-1113 Sofia, Bulgaria
43 Center for High Energy Physics, Adv. Inst. of Sciences and Technology, 305-701 Taejon, Republic of Korea
44 University of Alabama, Tuscaloosa, AL 35486, USA
45 Utrecht University and NIKHEF, NL-3584 CB Utrecht, The Netherlands
46 Purdue University, West Lafayette, IN 47907, USA
47 Paul Scherrer Institut, PSI, CH-5232 Villigen, Switzerland
48 DESY-Institut für Hochenergiephysik, D-15738 Zeuthen, FRG
49 Eidgenössische Technische Hochschule, ETH Zürich, CH-8093 Zürich, Switzerland
50 University of Hamburg, D-22761 Hamburg, FRG
51 National Central University, Chung-Li, Taiwan, China
52 Department of Physics, National Tsing Hua University, Taiwan, China
 § Supported by the German Bundesministerium für Bildung, Wissenschaft, Forschung und Technologie
 ‡ Supported by the Hungarian OTKA fund under contract numbers T019181, F023259 and T024011.
 ¶ Also supported by the Hungarian OTKA fund under contract numbers T22238 and T026178.
 ♭ Supported also by the Comisión Interministerial de Ciencia y Technología.
 ♯ Also supported by CONICET and Universidad Nacional de La Plata, CC 67, 1900 La Plata, Argentina.
 ♮ Supported by Deutscher Akademischer Austauschdienst.
 ◇ Also supported by Panjab University, Chandigarh-160014, India.
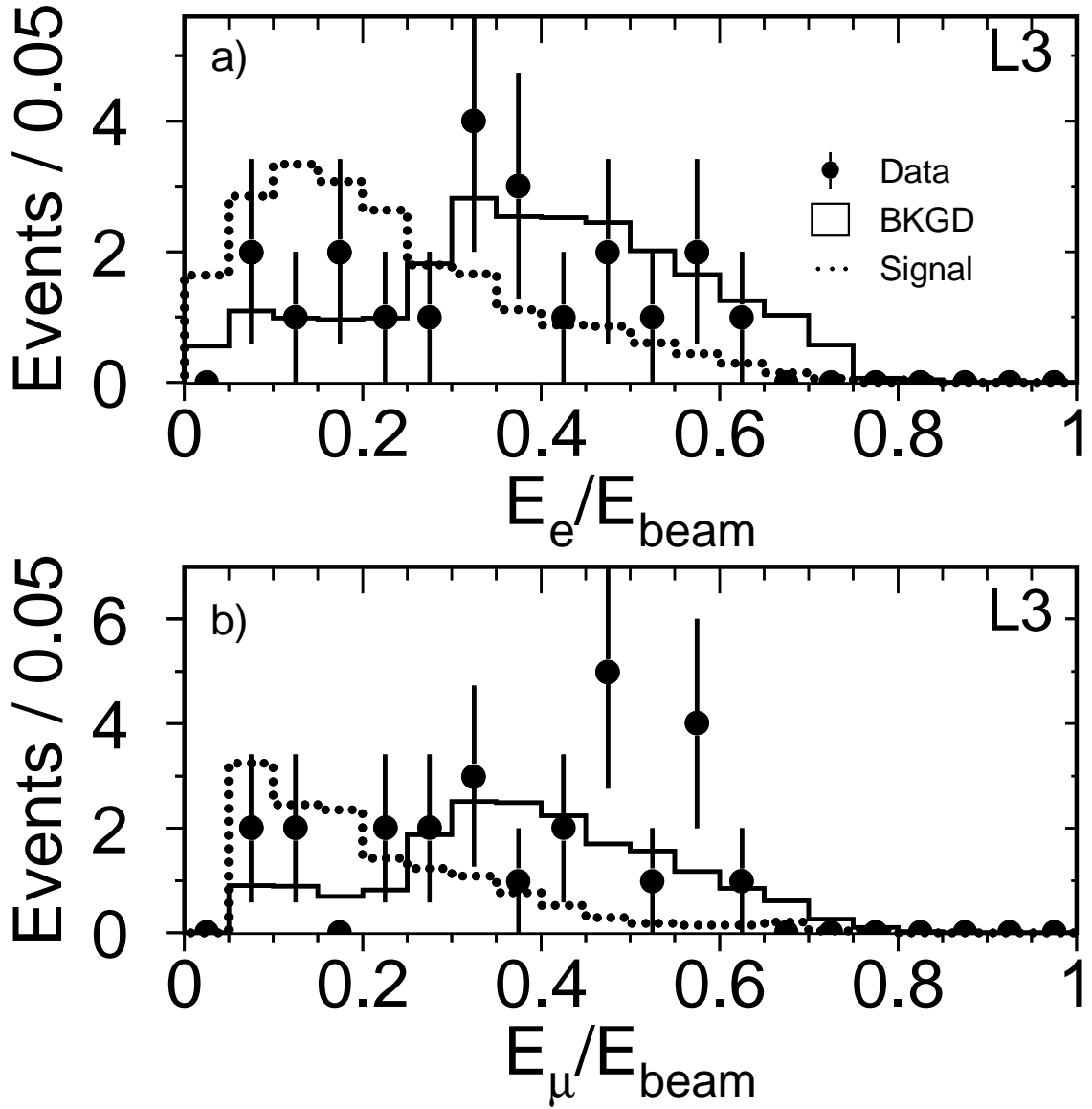 △ Supported by the National Natural Science Foundation of China.

Figure 1: Energy spectra, after pre-selection, for events with (a) electrons and (b) muons in the final state for $\sqrt{s} = 183$ GeV. The dotted line indicates the signal of a 60 GeV charged Higgs boson at $\mathrm{Br}(\mathrm{H}^{\pm} \to \tau\nu) = 1$ multiplied by a factor 5. The background is dominated by W decays into leptons.
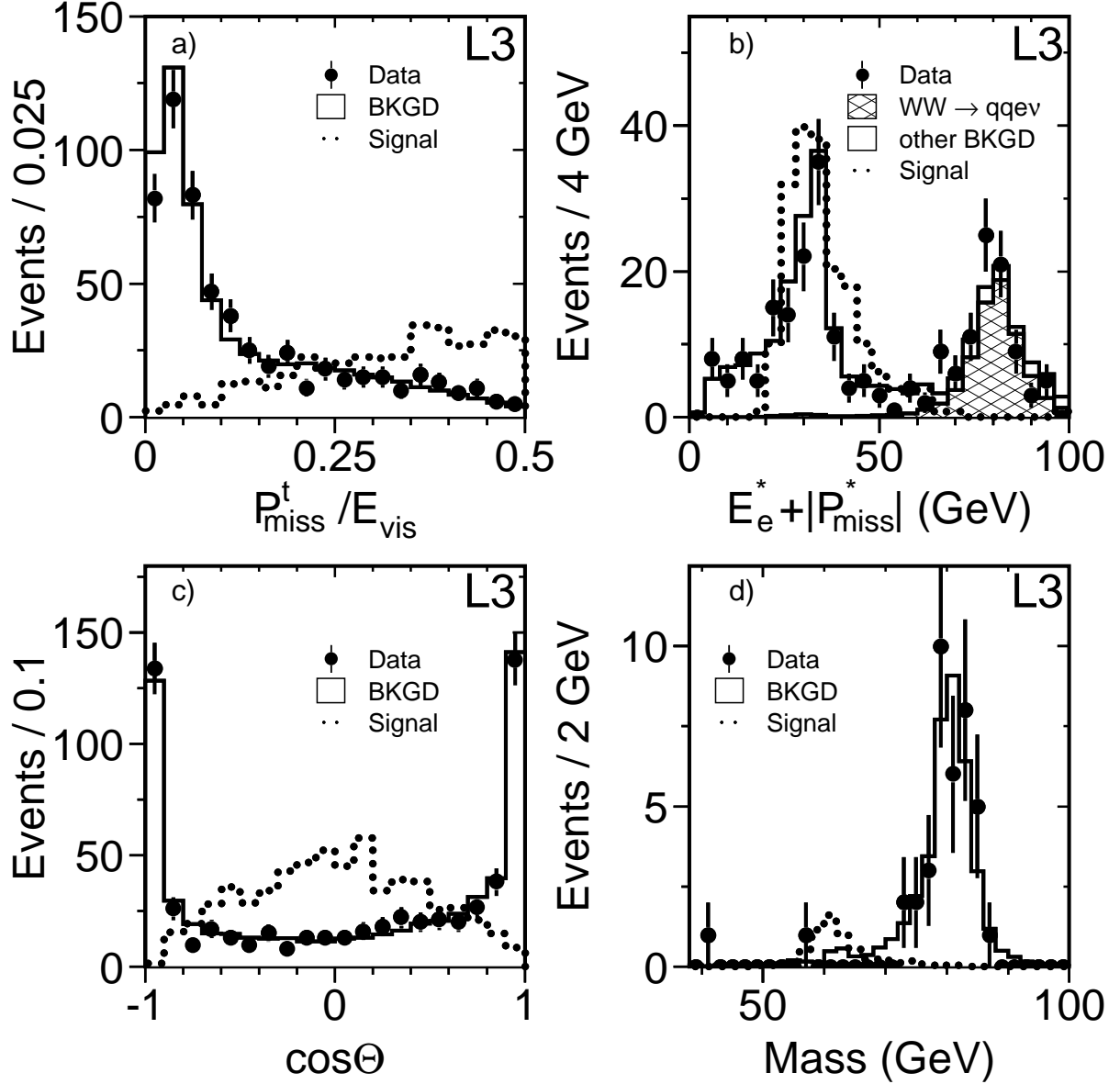
Figure 2: Distributions for the $H^+H^- \to c\bar{s}\tau^-\bar{\nu}_\tau$ channel after the pre-selection and the τ identification: a) ratio of the missing transverse momentum and the visible energy for $\sqrt{s} = 183$ GeV, b) sum of the electron energy and the absolute value of the missing momentum in the rest frame of the leptonically decaying parent particle for events with an identified electron in the final state for $\sqrt{s} = 183$ GeV, the background process $W^+W^- \to q\bar{q}e\nu$ is clearly separated from the signal, c) polar angle distribution of the negative parent particle for $\sqrt{s} = 183$ GeV, d) reconstructed mass spectrum after all cuts for $\sqrt{s} = 130 - 183$ GeV. The dotted lines indicate the signal for a 60 GeV charged Higgs boson at $Br(H^\pm \to \tau\nu) = 0.5$ multiplied by a factor 100 (a-c) and by a factor one (d).
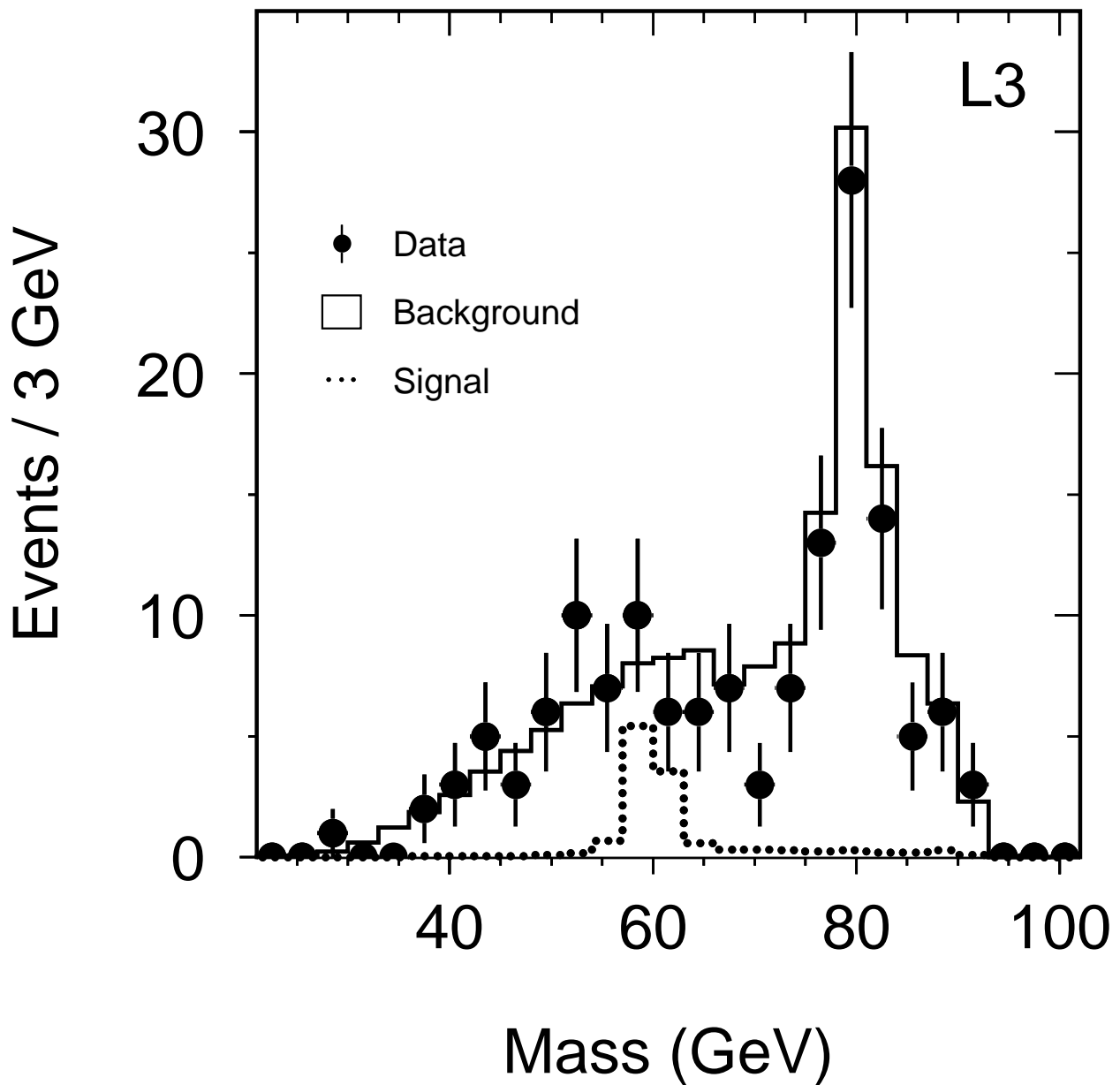
Figure 3: Distribution of the mass resulting from a kinematic fit, with assumed production of a pair of equal mass particles, for data and background events in the $c\bar{s}\bar{c}s$ channel at $\sqrt{s} = 130 - 183$ GeV. The dotted line indicates the signal of a 60 GeV charged Higgs boson at $Br(H^{\pm} \to cs) = 1$.
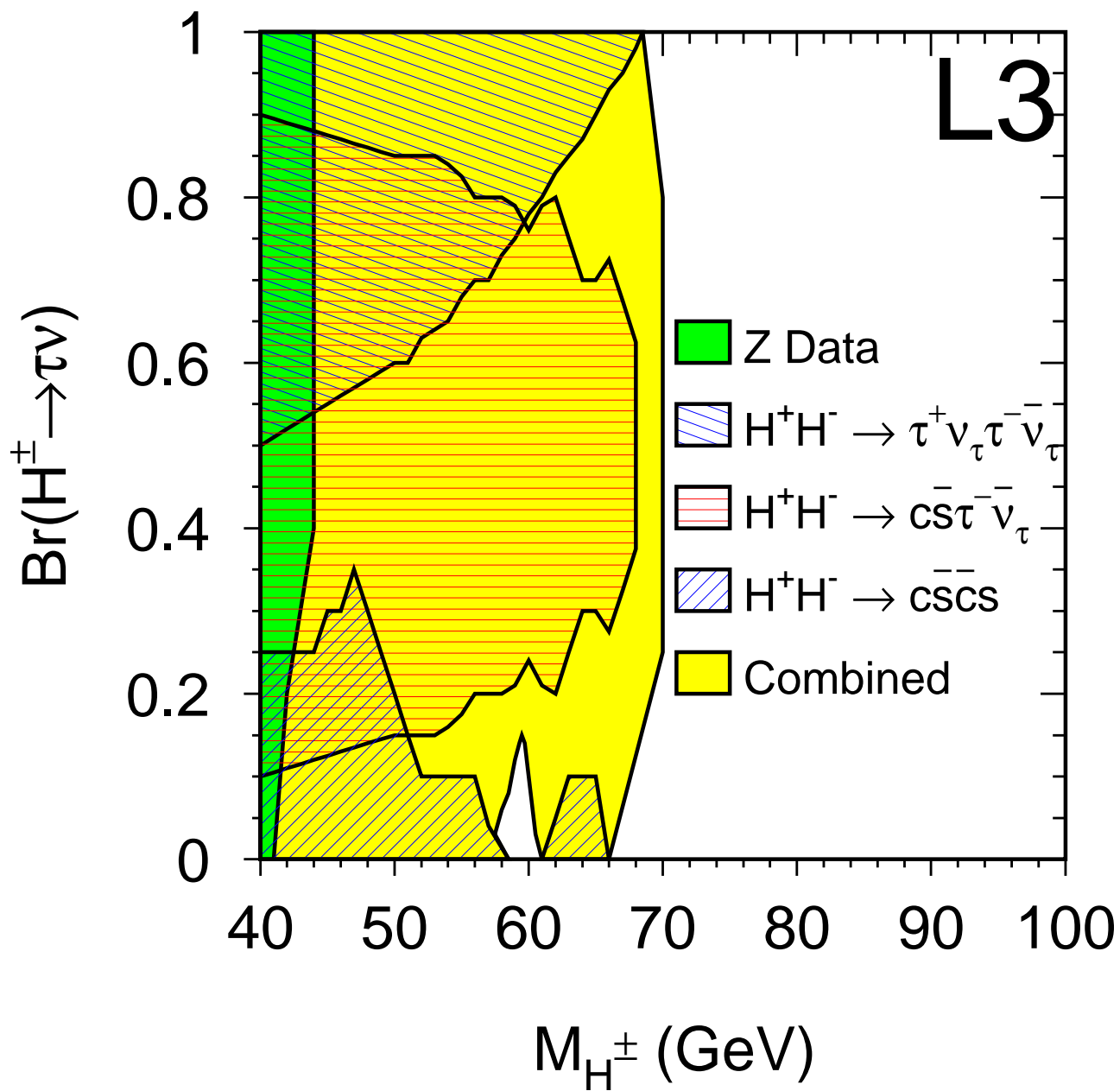
Figure 4: Excluded regions for the charged Higgs boson at 95% CL in the plane of the branching fraction Br(H$^\pm \to \tau\nu$) versus mass.